THE JOURNAL OF PHYSICAL CHEMISTRY A

Article

pubs.acs.org/JPCA

Driving Force Dependence of Charge Recombination in Reactive and Nonreactive Solvents

Arnulf Rosspeintner,[†] Gonzalo Angulo,[‡] and Eric Vauthey*[,†]

[†]Department of Physical Chemistry, University of Geneva, CH-1211 Geneva, Switzerland

[‡]Institute of Physical Chemistry, Polish Academy of Science, 01-224 Warsaw, Poland

Supporting Information

ABSTRACT: This study addresses the free energy dependence of charge recombination following photoinduced bimolecular electron transfer in three different solvents of either inert (acetonitrile and benzyl acetate) or reactive (*N*,*N*-dimethylaniline) character. Femtosecond time-resolved fluorescence and transient absorption have been used to determine the time scales for charge recombination. In pure *N*,*N*-dimethylaniline, charge recombination is found to be substantially slower than charge separation in a range of driving forces covering 1.5 eV. In all three solvents, the so-called Marcus inverted region is clearly observed for charge recombination. Additionally, the charge recombination step is found to be influenced by the solvent relaxation dynamics. A diffusion-reaction equation approach using an electron transfer model accounting for solvent relaxation is used to rationalize the experimental results.

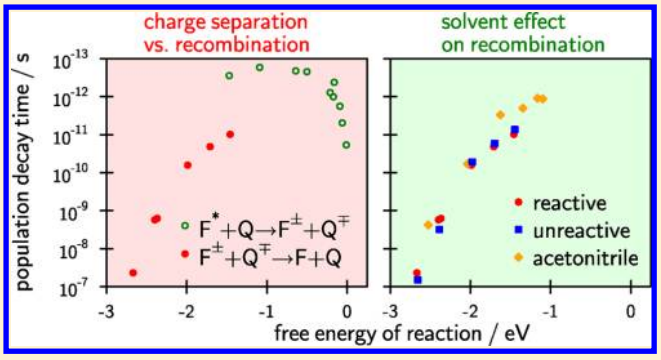

INTRODUCTION

The elucidation of the relevant factors governing electron transfer reactions, such as the driving force of the reaction or static and dynamic solvent properties, has been of significant importance for theoreticians[1−8] as well as experimentalists.[9−13] The initial theoretical formulation,[1] which, among other features, predicted a bell-shaped dependence of the rate on the driving force, has received numerous modifications and extensions. The inclusion of quantum modes and thus nuclear tunneling[3,14] allowed for a satisfying description of the temperature and driving force dependence of electron transfer.[4,11] Extending the theory to also account for the dynamic properties of the solvent[5,6,8,15] allowed the rationalization of many of the observed solvent and temperature dependences of mostly intramolecular charge transfer reactions.[16] Given this powerful arsenal of theoretical tools, most of the experimental observations could be rationalized. The predicted inverted region has eventually been observed in intramolecular charge separation reactions[11,17] and for many intermolecular charge recombination reactions.[18−20] Nonetheless, a clear-cut observation of the inverted region in diffusive intermolecular charge separation reactions is still lacking, and this fact has been given various explanations.[10,21,22]

The fact that charge separation and recombination, on the one hand, and intra- and intermolecular electron transfer, on the other hand, have resulted in, even qualitatively, different observations is striking and is yet lacking a general explanation. Studies on intermolecular electron transfer hold the intrinsic inconvenience that the charge transfer step itself is usually masked by the diffusional phenomena necessary to bring the reactants in close contact.[21,23,24] Intramolecular electron transfer does not suffer from this limitation, but holds the inconvenience that the relative spatial and orientational position of the donor and acceptor is relatively restricted.[25−27] An interesting experimental alternative to overcome both limitations has been put forward by investigating electron transfer reactions in neat electron-donating solvents.[28−30] Here, the reaction partners are not linked and restricted in their relative mutual orientation, whereas the translational diffusional approach of the reaction partners can evidently be assumed to be only of minor importance as the solvent actually is one of the reaction partners. Charge separation in pure aniline derivatives has been studied systematically by various groups focusing on the driving force dependence,[28] isotope[31] and substituent effects,[28] and reaction anisotropy.[30,32] The most important experimental finding that fluorescence quenching proceeds significantly faster than solvent relaxation and with mostly nonexponential kinetics has been rationalized either by recurring to a two-dimensional description of the electron transfer dynamics[28] or by invoking a distribution of reaction partners of different reactivity.[30,32]

Studies of the charge recombination of ion pairs in pure donating solvents are a bit scarcer and are usually limited to one or two systems, thus not allowing for significant conclusions when it comes to driving force effects.[29,33−40] As a consequence, the findings have been rather ambiguous so far. Whereas our group had found "inverted Marcus" behavior

Received: July 4, 2012
Revised: August 14, 2012
Published: August 15, 2012

   dx.doi.org/10.1021/jp306629v | *J. Phys. Chem. A* 2012, 116, 9473−9483

Chart 1. Electron Acceptors and Solvents, Including the Electron Donor (DMA)

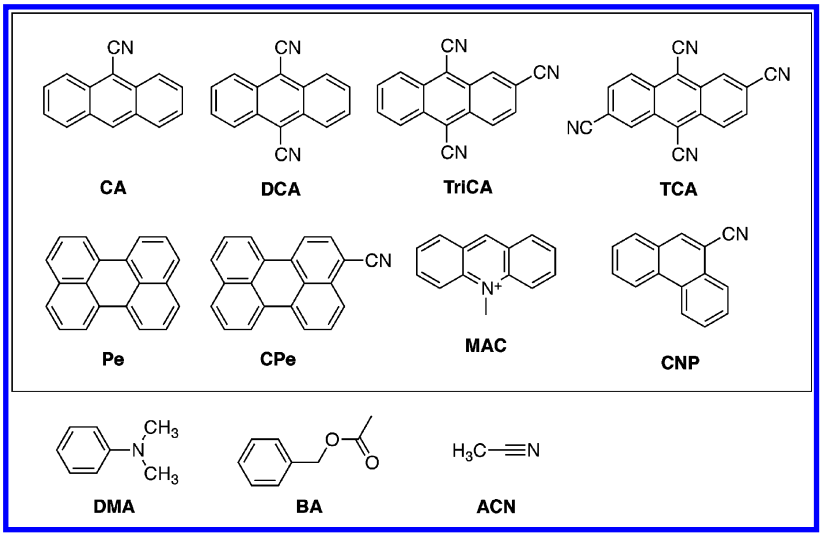

by comparing the charge recombination for two different reactant pairs,[41] Nibbering and co-workers had come to the opposite conclusion using a set of three reactant pairs.[40] In the latter paper, the authors had attributed their finding to steric effects.

The aim of this work is to answer the following questions: Are the time scales for charge separation and charge recombination in a pure donating solvent similar or not? Is there a significant difference for charge recombination when using a pure donating solvent and an inert solvent of otherwise similar physical properties? Do the dynamic properties of the solvent influence the charge recombination reaction? To this end, we have analyzed the charge recombination dynamics of a well chosen set of reactant pairs (Chart 1), spanning a sufficiently wide energy range of almost 1.5 eV, in three different solvents: acetonitrile, because it represents the model solvent for electron transfer reactions, *N*,*N*-dimethylaniline (DMA), as it is a reactive, electron-donating solvent, and has already been extensively used for investigations of charge separation reactions, and benzyl acetate, as it can be viewed as the unreactive analogue of DMA, having almost identical macroscopic solvent properties but not possessing the strong electron-donating ability (Table 1). To obtain a quantitative understanding of the experimental results, we have applied a diffusion-reaction equation formalism with various models for electron transfer.

EXPERIMENTAL SECTION

Chemicals. Benzyl acetate (BA, ACROS 99+ %) was used as received. *N*,*N*-Dimethyl-aniline (DMA, Aldrich, 99%) was distilled under reduced pressure and stored in the dark under argon. Perylene (Pe) was purified by sublimation. 9-Cyano-anthracene (CA) and 9,10-dicyano-anthracene (DCA, Kodak) were recrystallized. 2,9,10-Tricyano-anthracene (TriCA) and 2,6,9,10-tetracyanoanthracene (TCA) were synthesized as described in ref 42. Coumarin 481 (C481, Exciton) was used as received.

Spectroscopy. The experiments were performed with the fluorophores (10^{-5} to 5×10^{-4} mol/L, for steady-state and time-resolved experiments, respectively) in either BA with 1 mol/L DMA or pure DMA. Steady-state absorption and emission spectra were recorded on a Cary50 absorption spectrometer and a Cary Eclipse fluorimeter, respectively. The emission spectrum of C481 used for the reconstruction of the time-resolved emission spectrum in the evaluation of the solvent response time was recorded on a FluoroLog-3 fluorimeter. All fluorescence spectra were corrected for the spectrometer response.[43] Subnanosecond time-resolved emission measurements, with an approximate time resolution of 200 ps, were performed with a home-built time-correlated single photon counting (TCSPC) setup using a 395 nm laser diode (LDH-P-C-405 from Picoquant) as excitation source.[44]

Femtosecond time-resolved fluorescence measurements were carried out with a fluorescence up-conversion (FU) setup described already in ref 41. Excitation was performed at 400 nm using the frequency-doubled output of a Kerr lens mode-locked Ti:Sapphire laser (Mai Tai, Spectra-Physics). Excitation of the sample, contained in a spinning cell with 0.45 mm path length, was performed after adjusting the angle between pump and the gate pulses at 800 nm to magic angle. Eventually, the up-converted signal was focused into a monochromator (bandpass of 10 nm, corresponding to roughly 25 nm at the emission wavelength) equipped with a photomultiplier tube (Hamamatsu R1527P) working in photon counting mode at the exit slit. The full width at half-maximum (fwhm) of the overall instrument response function amounted to 250 fs.

Femtosecond transient absorption spectra were obtained using an apparatus described in refs 45, 46. The instrument response function has a full width at half-maximum of approximately 200 fs as obtained from measurements of the optical Kerr effect in BA and DMA. For the measurements in pure DMA, a 2 mm cuvette with water was brought in the pump beam to reduce two-photon absorption of DMA. The pump power at 400 nm was of the order of 1 mW. The sample absorbance at 400 nm was of the order of 0.5 in a 1 mm quartz cuvette. Samples were bubbled during the experiment with nitrogen to constantly refresh the excitation volume, thus avoiding sample decomposition. Changes in the sample concentration due to degradation and/or solvent evaporation were negligible as judged from absorption spectra before and after the experiments.

RESULTS

Figure 1 shows a schematic energy diagram for the electron transfer processes relevant for this investigation. Photoexcitation of the fluorophore (F) results in a locally excited fluorophore

dx.doi.org/10.1021/jp306629v | J. Phys. Chem. A 2012, 116, 9473−9483

Table 1. Solvent Properties at 20 °C

	E^{ox} (V, SCE)	η^a (cP)	ε^b	$n_D{}^c$	$\tau_L{}^d$ (ps)
DMA	0.7[e]	1.35	4.97	1.5582	15
BA		2.32	5.1	1.5232	10.7
ACN		0.37	35.9	1.3441	0.26

[a]Dynamic viscosity from ref 61. [b]Dielectric constant from ref 61. [c]Refractive index from ref 61. [d]Longitudinal solvent relaxation time: DMA from ref 31; the solvent relaxation time of BA was obtained following the procedure outlined in ref 62. However, here a global fit with multiexponential functions is applied to the entire set of wavelength resolved emission decays; ACN from ref 62. [e]Oxidation potential of DMA in acetonitrile from ref 20.

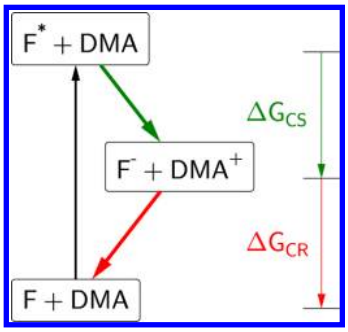

Figure 1. Energy level scheme pertaining to photoinduced charge separation (green, CS, from F*/DMA → F^-/DMA^+) and charge recombination (red, CR, from F^-/DMA^+ → F/DMA) and the associated driving forces.

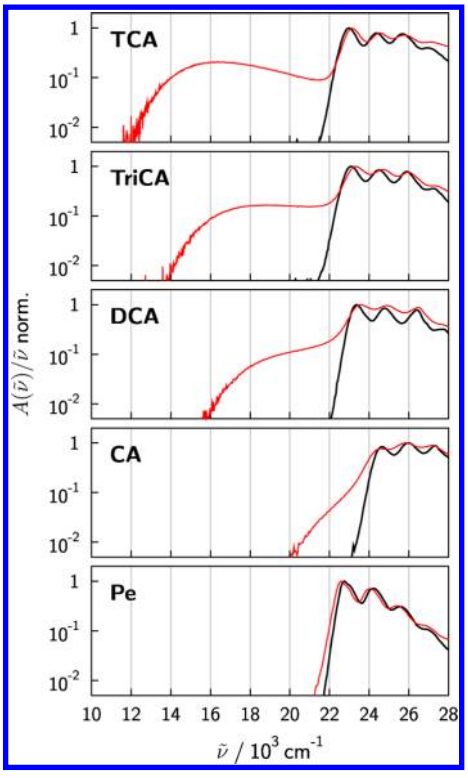

Figure 2. Normalized absorption spectra in transition dipole moment representation[55] of the electron acceptors in benzylacetate (black) and *N*,*N*-dimethyl-aniline (red).

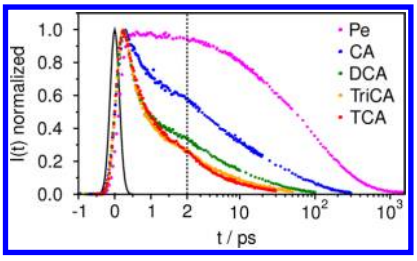

Figure 3. Femtosecond-resolved fluorescence decays measured with the various electron acceptors in BA with 1 mol/L DMA. Note the change from linear to logarithmic time scale at 2 ps.

(F*) that is a state where the excitation is localized on the fluorophore only, by contrast to exciplexes or charge transfer states, which can undergo charge separation (CS) with DMA giving rise to a radical ion pair (F^-/DMA^+). Alternatively, the charge-separated state can be populated directly by exciting into the corresponding charge transfer band. However, for the systems under investigation and the chosen excitation wavelength (400 nm), the direct charge transfer excitation is of minor importance (estimated to be always below 10%, cf., Figure 2). The locally excited-state population decay can be monitored spectroscopically by the disappearance of either its emission (F*) or absorption signature and indirectly via the appearance of the absorption of the produced ions. At the same time, the geminate ion pair can either diffusively separate into free ions or recombine, thus recovering the original educts (F, DMA).

Figure 3 shows the time profiles of the fluorescence intensities measured by FU with the different fluorophores in BA in the presence of 1 M DMA. They were analyzed using the analytical solution of the convolution of a Gaussian excitation pulse with multiexponential decays. The so-obtained mean lifetimes, $\tau_{CS} = \sum_i A_i\tau_i/\sum_i A_i$, are collected in Table 2. The fact that the decays are rather multi- than monoexponential can be attributed to two reasons: First, the quenching proceeds diffusionally at longer times, giving rise to the appearance of a so-called transient effect, that is, a time-dependent rate constant. Second, it has been observed that even in pure DMA, where no diffusion is required, reaction kinetics proceed non- or at least multiexponentially. The latter has been given different explanations comprising solvation effects[31] and to nonequilibrium dynamics.[30,32] In line with previous findings in pure DMA, the mean lifetimes show a distinct dependence on the driving force for charge separation. In particular, the reaction gets faster the larger is the driving force, in agreement with the fact that, for the present systems, charge separation occurs in the normal Marcus region. Except for Pe and CNPe, the charge separation dynamics were too fast to be reasonably resolved with the time-resolution of our up-conversion apparatus. However, these data are available from ref 47.

Figure 4a shows the baseline and chirp corrected experimental transient absorption spectrum of CA and 1 mol/L DMA in BA upon excitation at 400 nm. In the absence of DMA (Figure 4b), that is, CA in BA, the excited-state absorption, stimulated emission, and ground-state bleach of CA contribute to the observed spectra. Thus, obtaining the charge recombination dynamics from TA spectra is not completely straightforward, as the experimental spectra not only consist of the ion signatures (F^-/DMA^+), but also of these pure fluorophore features. In addition, as previously noted,[32] already pure DMA gives a small (<1 mOD) although observable residual transient signal, $A_{DMA}(t,\lambda)$, upon 400 nm excitation, most probably due to two-photon excitation (cf., Supporting Information). To obtain the pure ion kinetics, that is, without excited-state absorption and

dx.doi.org/10.1021/jp306629v | J. Phys. Chem. A 2012, 116, 9473−9483

Table 2. Experimental Time Constants for Charge Separation, CS, and Charge Recombination, CR

			τ_{CR}^{-1} (10^9 s^{-1})			τ_{CS}^{-1} (10^{12} s^{-1})		
	E^{red} (V, SCE)[a]	E_{00} (eV)[a]	ACN[a]	DMA	BA	ACN[a]	DMA	BA
MAC	−0.46	2.77	910			>5		
TCA	−0.45	2.82	870	102	137	>5	3.6	0.45
TriCA	−0.70	2.89	500	48	59	>5		0.38
DCA	−0.98	2.88	330	16	19	>5	5.9	0.24
CA	−1.39	2.96	17	0.58	0.32	>5	4.8	0.05
CPe	−1.36	2.60		0.62[b]			2.4[b]	
Pe	−1.66	2.83		0.023[b]	0.015		0.2[b]	0.007
CNP	−1.88	3.42	0.42			>5		

[a]From ref 20. [b]From ref 41.

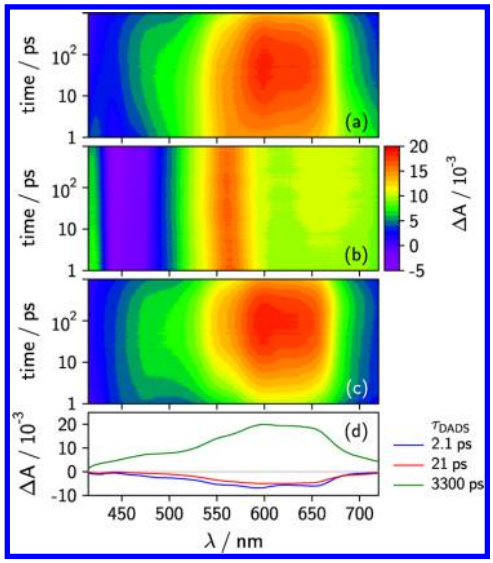

Figure 4. (a) Transient absorption spectra measured with CA in BA in the presence of 1 mol/L DMA, $A_{F,DMA}(t,\lambda)$, and (b) without DMA, $A_F(t,\lambda)$, upon excitation at 400 nm. (c) Pure ion kinetics, $P(t,\lambda)$, as defined by eq 1 and obtained from spectra (a), (b), and fluorescence up-conversion data. (d) Decay associated difference spectra (DADS) obtained from global analysis to the pure ion data of (c). Note that for better visibility the TA data were rounded to integer values in the surface plots. The spectrotemporal changes of the locally excited fluorophore can be clearly observed in (b).

stimulated emission contributions from the locally excited fluorophore, and residual contributions from the solvent/quencher, we applied the following modification, which is exemplified in Figure 4:

$$P(t,\lambda) = A_{F,DMA}(t,\lambda) - A_{DMA}(t,\lambda)S_1 - A_F(t,\lambda)\frac{I_{F,DMA}(t,\lambda_{em})}{I_F(t,\lambda_{em})}S_2 \quad (1)$$

where $A_x(t,\lambda)$ are the transient absorption spectra of the F−DMA pair (F, DMA; Figure 4a), the pure fluorophore (F; Figure 4b), and the quencher solution (DMA), and $P(t,\lambda)$ denotes the spectrotemporal behavior of the ion pair (Figure 4c). $I_{F,DMA}(t,\lambda_{em})$ and $I_F(t,\lambda_{em})$ denote the emission decays of the locally excited fluorophore obtained from the fluorescence up-conversion experiment at an arbitrary emission wavelength, λ_{em}, in the presence and absence of DMA, respectively. S_1 is the scaling factor for the subtraction of the residual DMA contribution upon direct DMA excitation. It was chosen such that the characteristic signal for DMA (as measured using either only pure DMA or 1 M DMA in BA) at long times, where no contribution from the ions was observable, vanished. S_2 denotes a scaling factor, accounting for fluctuations in the laser intensity and changes in the sample absorbance at the excitation wavelength in the experiments for $A_{F,DMA}$ and A_F. Obviously, this method can only be applied for time delays exceeding the instrument response function, as convolution is not accounted for. Therefore, the data starting from 500 fs or 1 ps in BA and DMA are analyzed, respectively. As the educt contributions to the TA spectra had vanished within 500 fs to 1 ps for most of the acceptors in pure DMA (except for Pe and CNPe), it was not necessary to apply eq 1, and only the correction for the DMA contribution had to be performed. Eventually, a parallel kinetic model for 2 to 3 species was globally fitted to $P(t,\lambda)$ using an algorithm proposed in ref 48. For the charge recombination step, only the lifetime of the so-obtained decay associated difference spectra with significant positive amplitudes was taken. Those with negative amplitudes can be attributed either to the rise of the ion signal or to slight variations in the ion band shape at short times. Eventually, all ion decays could be reasonably well reproduced by a monoexponential decay. These ion pair lifetimes, τ_{CR}, which correspond to the charge recombination dynamics, are summarized in Table 2. Figure 5 shows the transient absorption spectra of the "pure" ion pair and compares them to the spectra of the individual ions obtained either chemically, electrochemically, or via pulse radiolysis. The important spectral features clearly show that indeed the ions are being formed and monitored in our experiment. The slight differences in the spectral features and position can be attributed to the different solvents used in our experiments and those for the individual ions.

For the cases where the recombination kinetics were of the order of 2 ns (the maximum time range observable by TA) or slower, the lifetimes extracted from transient absorption data become unreliable. However, for all of the relevant systems, that is, CA, Pe, and CNPe in BA and CA in pure DMA, an exciplex (contact radical ion pair) emission band at longer wavelengths than the locally excited-state emission was observable. The CR dynamics was thus determined from the decay of this emission using TCSPC. This presents a feasible alternative for low polarity solvents, such as BA and DMA, as the low dielectric constant and thus the Coulomb attraction of the ions renders escape to free ions virtually impossible. At higher dielectric constants and/or low viscosities (such as in acetonitrile), the exciplex kinetics would be governed by the complex interplay of charge recombination and diffusive separation of the geminate ion pair.[49] In this case, the exciplex kinetics cannot and have not been taken as equivalent to those of the ion pair.[20]

dx.doi.org/10.1021/jp306629v | J. Phys. Chem. A 2012, 116, 9473−9483

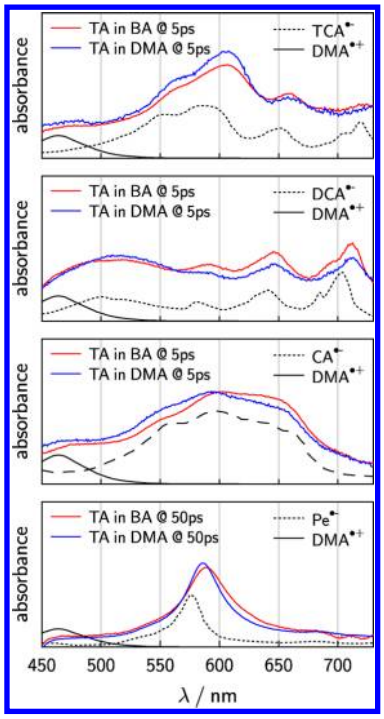

Figure 5. Comparison of the "pure ion" spectra obtained from the transient absorption data (in BA and DMA) with the absorption spectra of the individual ions, obtained either chemically, electrochemically, or by pulse radiolysis. DMA^+, Pe^-, and TCA^- in acetonitrile are taken from refs 63, 64, and 65, respectively. CA^- and DCA^- in dimethylformamide are taken from refs 66 and 67.

DISCUSSION

To have a more comprehensive data set for comparison, previously published[20] data for charge recombination in ACN were added to the analysis. The therein published data had been recorded using the transient grating technique, and the corresponding ion population decays were found to be monoexponential. For the charge separation data in ACN, no representative lifetimes are published; however, it is noted in ref 20 that the ions were formed within the instrument response function of the apparatus (laser pulse width of the laser of 120 fs). We can complement Table 2 by adding this data set to those obtained in the present work. Figure 6 graphically summarizes the results from two perspectives: first, the comparison between charge separation and charge recombination time scales in pure DMA (Figure 6a), and, second, the charge recombination dynamics in the three different solvents (Figure 6b). We shall start by giving a purely qualitative account of the experimental findings.

Charge Recombination versus Charge Separation in DMA. Figure 6a depicts the different time scales for charge separation and charge recombination in neat DMA (see also Table 2). Note that the plot merely serves to compare relevant time scales and not rate constants. Indeed charge separation and recombination reactions are intrinsically different insofar, as the charge separation step is a bimolecular (concentration-dependent) process, while the recombination reaction is a purely geminate (concentration-independent) process. Nonetheless, even from the mere inspection of the experimental time scales, one can extract valuable information. At first sight, three observations can be made:

(1) Both charge separation and recombination show distinct driving force dependences. In the case of charge separation, this dependence has been reproduced quantitatively by Yoshihara and co-workers in ref 31 using an electron transfer model developed by Marcus and Sumi, which accounts for faster-than-solvation electron transfer.[6] The observed driving force dependence for charge recombination in neat DMA shows the clear-cut presence of the Marcus inverted region, which is contrary to the findings in ref 40, where no such dependence had been found.

(2) The fastest observed charge separation in pure DMA is by almost 2 orders of magnitude faster than the fastest observed charge recombination.

(3) As a guide to the eye, we have tentatively included the mean longitudinal solvent relaxation time of DMA and its components in the plot. By mere inspection of Figure 6a, one is tempted to state that charge recombination seems to be under solvent control, while the same is not true for charge separation.

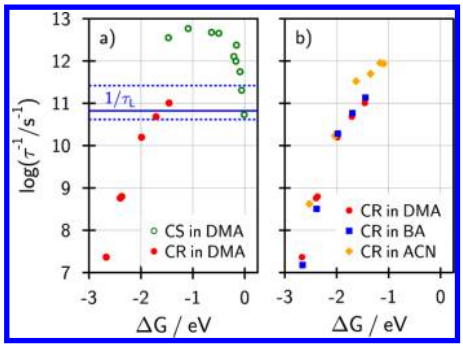

Figure 6. (a) Free energy dependence of the inverse charge separation (green ○) and ion recombination (red ●) time constant in pure *N*,*N*-dimethylaniline. The data for the charge separation were taken from refs 31 (coumarines), 47 (cyanoanthracenes), and 30 (Pe and CNPe). Additionally, the mean solvent relaxation time (full blue line), as measured from dynamic Stokes shift experiments, and its components (dotted blue lines) are indicated. (b) Free energy dependence of charge recombination in *N*,*N*-dimethylaniline (red ●), benzyl acetate (blue ■), and acetonitrile (orange ◆).

Charge Recombination in Different Solvents. Figure 6b shows a comparison of the relevant time scales of charge recombination in the three different solvents studied. Again, we can list the most notable observations:

(1) Charge recombination in the two viscous solvents of low dielectric constant, BA and DMA, proceeds virtually identically. It is thus interesting to note that the radical pair, once generated upon photoinduced electron transfer, does not care whether it is surrounded by inert solvent molecules (BA) or neutral reaction partners (DMA). This is a clear indication that hole hopping in pure DMA is absent or at least not of crucial importance. Additionally, this observation denotes the pure pairwise nature of the recombination process.

(2) The maximum value of the inverse lifetime is by almost 1 order of magnitude larger in ACN than in BA or DMA. This observation leads us to invoke effects of the longitudinal solvent relaxation time, τ_L, on the dynamics. Here, we do not take into account changes in the absolute value of the coupling matrix element, V, which is supposed to be a mere property of the reactants and thus solvent independent. Obviously, τ_L only becomes strikingly important for solvent-controlled (i.e., outer sphere) electron transfer.

dx.doi.org/10.1021/jp306629v | J. Phys. Chem. A 2012, 116, 9473−9483

We will proceed by leaving behind qualitative interpretations or oversimplified models, which do not take into account the complex interplay of generation and disappearance of ions, and will rather attempt to reproduce the entire data set of CR time constants.

SIMULATIONS

To obtain a more realistic description of bimolecular processes in solution, it is necessary to apply diffusion-reaction models. Moreover, if the reaction step of interest is the follow-up reaction of a previous diffusion influenced reaction, it is mandatory to apply a set of coupled diffusion-reaction equations. One may argue that, in low polarity high viscous solvents, diffusion is of minor importance for the charge recombination as the geminate radical ion pair will hardly leave the Coulombic potential well and thus remain inside the sphere defined by the Onsager radius (approximately 140 Å at $\varepsilon = 5$). However, in low viscous polar solvents, such as acetonitrile, this simple assumption definitely does not hold. Thus, to compare kinetics in DMA and BA with those in acetonitrile, the same analysis should be applied to all data for reasons of consistency. In this section, we will outline the general diffusion-reaction approach, then focus on the different models that can be used as sink, that is, reaction terms, and eventually present the simulation/fitting results.

Diffusion-Reaction Approach. This approach has already been applied to similar problems[29,50,51] and has been recently reviewed.[21] Two diffusion-reaction equations describing the spatio-temporal evolution of the reactant, $n(r,t)$, and product, $m(r,t)$, pair distribution functions are required for the following process:

$$\mathrm{F} + \mathrm{DMA} \xrightarrow{h\nu} \underbrace{\mathrm{F}^* + \mathrm{DMA}}_{n(r,t)} \xrightarrow{\mathrm{CS}} \underbrace{\mathrm{F}^- + \mathrm{DMA}^+}_{m(r,t)} \xrightarrow{\mathrm{CR}} \mathrm{F} + \mathrm{DMA} \tag{2}$$

Note that both charge separation and charge recombination are assumed to be irreversible. This is a solid assumption given the fact that the driving force for all processes under consideration is always larger than 0.3 eV. In line with the findings in ref 29, charge diffusion is described by material transport; that is, hole hopping from DMA^+ to DMA is not included. Only geminate processes are taken into account for the separated charges, given that the acceptor concentration is rather low (at most in the range of 10^{-5} mol/L).

$$\frac{\partial n(r,t)}{\partial t} = \hat{L}_{\mathrm{CS}}(r)n(r,t) - w_{\mathrm{CS}}(r)n(r,t) \tag{3}$$

$$\frac{\partial m(r,t)}{\partial t} = \hat{L}_{\mathrm{CR}}(r)m(r,t) - w_{\mathrm{CR}}(r)m(r,t) + w_{\mathrm{CS}}(r)n(r,t)N(t) \tag{4}$$

Here, the subscripts CS and CR refer to charge separation and charge recombination, respectively. The following boundary and initial conditions are applied:

$$n(r,0) = g(r) \qquad \frac{\partial n(\sigma,t)}{\partial r} = 0 \qquad n(\infty,t) = 1$$

$$m(r,0) = 0 \qquad \frac{\partial m(\sigma,t)}{\partial r} = 0$$

Here, $g(r)$ denotes the solvent−solvent pair distribution function, calculated for hard spheres using the Percus-Yevick equation, and σ is the contact radius. The experimental observables are the reactant, $N(t)$, and product, $P(t)$, time dependences:

$$N(t) = N(t=0)\exp\left(-\frac{t}{\tau_0} - c\int_0^t k(t')\,\mathrm{d}t'\right) \tag{5}$$

$$P(t) = c4\pi\int_\sigma^\infty m(r,t)r^2\,\mathrm{d}r \tag{6}$$

c denotes the DMA concentration, and τ_0 is the fluorophore lifetime. It is worthwhile mentioning that the concentration dependences of $N(t)$ and $P(t)$ are distinctly different. While the decay of $N(t)$ will strongly be altered by changing the concentration, the changes in $P(t)$ are much more subtle. The quencher concentration, c, "only" scales the product kinetics; however, indirectly, it has more subtle and less straightforward effects via the generation of the ions and their initial resulting distribution. In other words, it is possible to extract a concentration-independent, however, time-dependent, quenching rate coefficient, $k(t)$, for charge separation. The same is not true for charge recombination.

The following definitions are required:

$$k(t) = 4\pi\int_\sigma^\infty w_{\mathrm{CS}}(r)n(r,t)r^2\,\mathrm{d}r \tag{7}$$

$$\hat{L}_x(r) = \frac{1}{r}\frac{\partial}{\partial r}D(r)\exp(-\nu_x(r))\frac{\partial}{\partial r}\exp(\nu_x(r)) \tag{8}$$

where in the case of charge separation $\nu_{\mathrm{CS}}(r) = -\ln(g(r))$ and in the case of recombination $\nu_{\mathrm{CR}}(r) = -\ln(g(r)) + r_{\mathrm{C}}/r$, with r_{C} denoting the Onsager radius of the Coulombic well. D denotes the distance-dependent mutual diffusion coefficient of the reactants and is given by[52]

$$D(r) = \frac{4k_{\mathrm{B}}T}{6\pi\eta\sigma}\left(1 - \frac{3\sigma}{4r}\right) \tag{9}$$

Models for Electron Transfer. The different model functions for the sink terms, w_x, in eqs 3 and 4 shall be introduced now. The semiclassical Marcus expression,[3,4,14] Jortner's and Bixon's extension accounting for the solvent dynamic effect[15] originally introduced by Zusman,[5] and a simplification[53] of Barbara's modification[16] of Sumi's and Marcus' two-dimensional model for electron transfer were used.[6] Figure 7 gives a schematic illustration of these electron transfer models.

- Semiclassical Marcus (model I): In addition to the classically treated solvent modes, which constitute the distance-dependent solvent reorganization energy, $\lambda_s(r)$, a generalized vibrational mode is treated quantum mechanically (i.e., $\hbar\omega \gg k_{\mathrm{B}}T$), having a reorganization energy λ_{qm}. By doing so, nuclear tunneling as well as the possibility of a reaction to vibrationally excited products are included.

$$w_x(r) = \sum_{n=0}^{n=\infty} U(r)\mathrm{e}^{-S}(S^n/n!) \times \exp\left(-\frac{(\Delta G_x(r) + \lambda_s(r) + \hbar\omega n)^2}{4k_{\mathrm{B}}T\lambda_s(r)}\right) \tag{10}$$

$$U(r) = \frac{V(r)^2}{\hbar}\sqrt{\frac{\pi}{k_{\mathrm{B}}T\lambda_s(r)}} \tag{11}$$

$$V(r) = V\exp\left(-\frac{r-\sigma}{L}\right) \tag{12}$$

$$S = \lambda_{\mathrm{qm}}/\hbar\omega \tag{13}$$

dx.doi.org/10.1021/jp306629v | J. Phys. Chem. A 2012, 116, 9473−9483

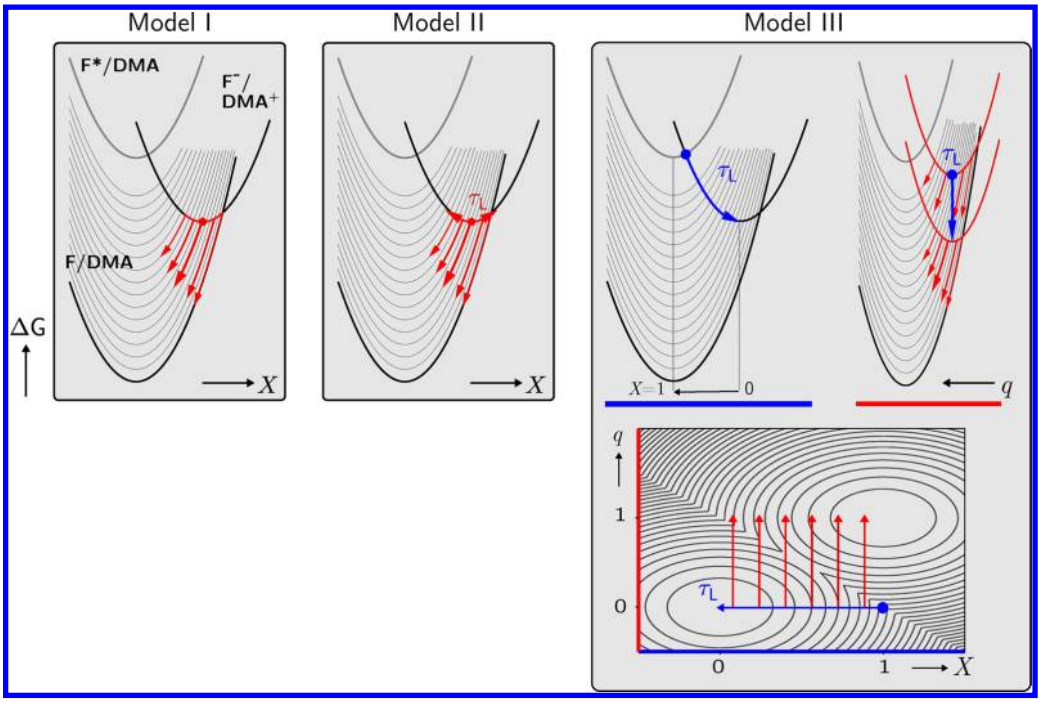

Figure 7. Schematic representation of the three electron transfer models. X and q refer to the classical solvent coordinate and classically treated intramolecular (not governed by solvent dynamics) coordinate. The quantum mechanically described vibrational mode is accounted for by the vertically displaced parabolas of the F/DMA free energy surface. τ_L denotes the longitudinal solvent relaxation time. In model II, τ_L directly influences the electron transfer rate by attenuating the amplitude of the various reaction channels (cf., eq 18). Its influence on the charge recombination in model III is conceptually different, as it introduces a time-dependent driving force due to the solvent-controlled relaxation of the ion pair, initially generated out of equilibrium.

Here, σ denotes the reactants' contact radius, V is the contact value of the coupling matrix element, and L is its decay length. The solvent reorganization energy is calculated according to

$$\lambda_s(r) = k\lambda_s^{M}(\sigma)\left(2 - \frac{\sigma}{r}\right) \tag{14}$$

$$\lambda_s^{M}(\sigma) = \frac{e^2}{4\pi\varepsilon_0\sigma}\left(\frac{1}{n^2} - \frac{1}{\varepsilon}\right) \tag{15}$$

where we have introduced a scaling factor k, to account for the fact that this estimation of the solvent reorganization energy tends to overestimate its actual value.[54] For λ_{qm}, a value of 0.28 eV as previously used in ref 20 was adopted. The driving force, ΔG_x, is defined as follows:

$$\Delta G_{CS}(r) = E(DMA^+/DMA) - E(F/F^-) - E_{00} + k_B T\frac{r_C}{r} \tag{16}$$

$$\Delta G_{CR}(r) = -E(DMA^+/DMA) + E(F/F^-) - k_B T\frac{r_C}{r} \tag{17}$$

CS and CR refer to the charge separation and recombination processes shown in eq 2. E are the reduction potentials taken from electrochemical measurements. E_{00} denotes the fluorophore 0–0 transition energy, obtained from absorption and fluorescence measurements as $E_{00} = h(\nu_a + \nu_f)/2$. Here, ν_a and ν_f denote the frequency of the lowest energy vibronic absorption peak and highest energy vibronic emission peak, respectively. To determine these energies, the spectra have been corrected for the instrument response[42] and transformed in the transition dipole moment representation, that is, $A(\lambda)/\nu$ and $I(\lambda)/\nu^5$.[5,55] When using DMA as solvent, no steady-state emission spectra were obtained, and the E_{00} values from BA were used. r_C is the Onsager radius given by $r_C = z_i z_j/(4\pi\varepsilon_0\varepsilon k_B T)$, with $z_{i,j}$ being the charge of the ions. One crucial point is whether the energy of the radical ion pair is properly described by eq 17. Using the position of the red edge of the charge transfer absorption band as the lower limit for the estimation of this energy, a very satisfying congruence between these values and those obtained using eq 17 can be found. We can thus safely assume that the driving force for the charge recombination step is sufficiently well described by eq 17 and that the coupling between reactants and products is sufficiently small not to significantly alter the $\Delta G_{CS/CR}$ values.

- Solvent dynamic effect (model II): The solvent dynamics is taken into account using an interpolation formula between the semiclassical Marcus expression and Kramers theory. Electron transfer is still assumed to proceed nonadiabatically; however, the motion of the reaction system along the free energy surface is now limited by the longitudinal solvent relaxation time, τ_L. Like in the semiclassical Marcus theory, the contributions to the reorganization energy are split into classical solvent modes, giving rise to $\lambda_s(r)$, and quantum mechanically treated vibrational modes, λ_{qm}. The final form of the distance-dependent reaction probability is given by

$$w(r) = \sum_{n=0}^{n=\infty} \frac{U(r)e^{-S}(S^n/n!)}{1 + \tau_s U(r)e^{-S}(S^n/n!)} \times \exp\left(-\frac{(\Delta G_x(r) + \lambda_s(r) + \hbar\omega n)^2}{4k_B T\lambda(r)}\right) \tag{18}$$

dx.doi.org/10.1021/jp306629v | J. Phys. Chem. A 2012, 116, 9473–9483

where

$$\tau_s = 4\tau_L\sqrt{\frac{\pi k_B T}{\lambda(r)}} \tag{19}$$

and all other parameters follow the above definitions.

- Barbara's hybrid model (model III): It is basically a combination of the two-dimensional Sumi−Marcus model including the quantum mode description of the semiclassical Marcus model. Here, the electron transfer system develops on a two-dimensional surface being spun by the classically treated solvent coordinate, X, and a low frequency classically treated intramolecular vibrational mode, q. In addition, one high frequency intramolecular vibration is treated quantum mechanically. Thus, one has three contributions to the reorganization energy $\lambda_s(r)$, λ_{cv}, and λ_{qm}. The dynamics of the solvent relaxation is in principle accounted for by letting the system relax along the X coordinate with the time constant being equal to the longitudinal solvent relaxation time, τ_L. Electron transfer itself proceeds almost exclusively along the q coordinate, that is, along the classic vibrational modes not associated to τ_L. Eventually, this description reduces to a time-dependent driving force for the electron transfer process, $\Delta G(r,t)$.

$$w(r,X) = \sum_{n=0}^{n=\infty} U(r)e^{-S}(S^n/n!) \times \exp\left(-\frac{(\Delta G(r,t) + \lambda_{cv} + \hbar\omega n)^2}{4k_B T\lambda_{cv}}\right) \tag{20}$$

where

$$\Delta G_{CR}(r,t) = \Delta G_{CR}(r) + \lambda_s(r)(1 - 2X(t)) \quad \text{with} \quad X(t) = X_0 e^{-t/\tau_L} \quad \text{and} \quad X_0 = 1 \tag{21}$$

λ_{cv} denotes the reorganization energy for the classically treated intramolecular vibrational modes ($\hbar\omega_{cv} \ll k_B T$). All other variables take on the above definitions.

The main difference between model III and the previous two resides in the fact that it accounts, albeit in a rather simplified way, for the nonequilibrium generation of the ions and their concomitant relaxation and reaction. Figure 7 gives a graphical account of these facts and a qualitative comparison of the factors governing charge recombination.

Results of the Analysis. As most of the ion population decays (disregarding the rise of the ion population) were well described by a monoexponential function, theory and experiment were compared by fitting the mean ion decay times calculated from eq 6 to the data in Table 2. In line with Fayer and co-workers[29] and for the very same reasons, our comparison between calculations and experimental data is only of semiquantitative character and intended for heuristic purposes. Its main aim consisted of finding, if possible, one representative parameter set for all solvents and reactant systems, showing that the observed trends can be properly explained by the chosen model. It is more than obvious that it will be impossible to obtain a perfect reproduction of the experimental kinetics with only one parameter set. Thus, a decent recovery of the mean time scale of the experiments using physically meaningful parameters and models seems to be a reasonable target. As a consequence, we were more interested in explaining the 5 orders of magnitude change in charge recombination and the difference in the various solvents, rather than obtaining a close to perfect reproduction of the dynamics of any of the individual systems.

The first point of interest concerns the simulation of the charge separation step. Fluorescence quenching reactions in pure DMA have been extensively studied,[30−32] and the observed ultrafast nonexponential kinetics have been explained using different theoretical approaches. Yoshihara and co-workers explained the faster-than-solvent-relaxation quenching applying the Sumi−Marcus model, whereas both the Castner group and our group ascribed it to distributions of quenchers with different reactivity. In any case, for the present study, the charge transfer step is only needed as a starting point for the charge recombination step. So far, we are not too much concerned about the intrinsic mechanisms causing nonexponential kinetics. As a consequence of the observed faster-than-solvation quenching dynamics and to keep things as simple as possible, the semiclassical Marcus model as a sink term in eq 3 was used, and no dynamic solvent effect on the generation of ions was considered. However, diffusional quenching, that is, by solving the diffusion-reaction equation for the quenching kinetics, was fully accounted for. As a matter of fact, satisfying results (comparing the simulated and experimental CS time, τ_{CS}) can be obtained using an electronic coupling matrix element of $V = 15 \pm 5$ meV and a decay length, L, of 2 Å.

The strategy for reproducing the charge recombination was as follows: Having obtained the parameters for charge separation, the recombination time constants, τ_{CR}, were analyzed using the full theoretical description outlined above, leaving only the coupling matrix element, V, and its decay length, L, as adjustable parameters. Additionally, the scaling factor in the solvent reorganization energy, k, was optimized as well. In model III, the reorganization energy of the classical intramolecular mode, λ_{cv}, was also adjusted. All other parameters were fixed to the values given in Table 3. These fixed values were taken either directly from experiments (macroscopic solvent properties) or from estimates reported in previous publications (values for λ_{qm} and $\hbar\omega$).[20]

Table 3 summarizes the best-fit parameters for the three different electron transfer models. From the global fits (i.e., analyzing all three solvent data with one parameter set simultaneously), the necessity of including $D(r)$ can not really be justified as the fit quality does not significantly improve upon inclusion of the hydrodynamic effect. However, in previous publications, its inclusion had been shown to be of mandatory importance for charge separation processes[56,57] and was thus used here in the individual fits as well. Comparison of the global parameter sets a and b favors the use of model III for various reasons:

- The residuals for model III are significantly smaller than those for models I and II.
- The L values for models I and II are significantly larger than those usually obtained for electron transfer reactions in liquid solution.[22,24,56−58]

However, we found that when grouping the solvents according to polarity and viscosity (i.e., taking DMA/BA as a set and ACN as another set), a significant improvement of the fitting could be achieved. The parameters of these fits to the two solvent subsets are different, reflecting a possible influence of the solvent on the parameters, which are thought to only reflect reactant intrinsic properties, V and L. Nonetheless, it seems justifiable that the different polarity and polarizability of

dx.doi.org/10.1021/jp306629v | J. Phys. Chem. A 2012, 116, 9473−9483

Table 3. Fitting Parameters for Charge Recombination in ACN, BA, and DMA

				parameters[a]				
model	$\lambda_s(r)$	$D(r)$	data set	V (meV)	L (Å)	k	λ_{cv} (eV)	res (s^{-1})
Ia	y	n	all	246	3.0	0.34		246
Ib	y	y	all	124	2.7	0.37		462
Ic	y	y	DMA/BA	34	2.7	0.99		25
			ACN	263	2.8	0.30		228
IIa	y	n	all	108	2.7	0.42		353
IIb	y	y	all	142	2.6	0.38		360
IIc	y	y	DMA/BA	79	2.8	1.00		44
			ACN	124	2.8	0.37		143
IIIa	y	n	all	102	2.1	0.36	0.16	150
IIIb	y	y	all	152	2.0	0.34	0.13	189
IIIc	y	y	DMA/BA	172	2.6	0.52	0.13	13
			ACN	124	1.9	0.41	0.10	119

[a]Additionally to these parameters, the following fixed values were used for all fits: σ = 6.9 Å, λ_{qm} = 0.28 eV, $\hbar\omega$ = 0.186 eV.[20] τ_L and η values were taken from Table 1. res denotes the goodness of fit and was calculated according to res = $\sum_i(1/\tau_{i,exp} - 1/\tau_{i,fit})^2\tau_{i,exp}$.

the solvent sets may have an effect on the electronic properties of the solutes. Models II and III yield now comparably good fits to the experimental data, while model I gives significantly worse fits (cf., Figure 8 and the Supporting Information

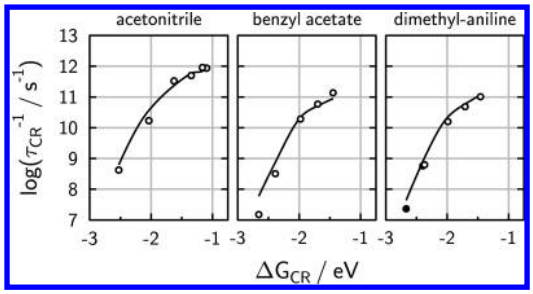

Figure 8. Free energy dependence of the inverse time constant for charge recombination of the ions. The lines depict the best fit of model IIIc (cf., Table 3).

for representative graphics). Nonetheless, as the discrepancies between the fitting parameters (e.g., k and V) for the two solvent sets are significantly larger for models I and II than for model III, this favors the latter over the former two. Summarizing, we can state that the obtained parameters for model III have reasonable values (although the L value for IIIc in DMA/BA is slightly larger than the usually assumed values of 2 Å),[56,59] with the electronic coupling matrix element being in the range of 100−150 meV, and its decay length being in the range of 2 Å. The values for V listed in Table 3 have to be taken with care, as actually the effective coupling matrix elements per reaction channel $V_{eff} = Ve^{-S}S^n/n!$ should be compared to data given in the literature. The so calculated maximal value of V_{eff} for the best fit with model III reduces to about 50 meV, which is only approximately $2k_BT$. Figure 8 shows the experimental data together with the result of the analysis with model IIIc, including $D(r)$, $\lambda_s(r)$. Thus, only the model that accounts for the nonequilibrium generation of the ions and the subsequent solvent-controlled relaxation is able to reasonably describe the free energy dependence of photoinduced charge recombination in three different solvents. In other words, charge recombination does not only occur from the ions in a relaxed solvent environment, but rather starts as soon as the ions are being formed. The recombination process itself is thus strongly influenced by the energetic relaxation of the ions.

CONCLUDING REMARKS

We have studied the driving force and solvent dependence of photoinduced charge recombination processes in liquid solution by femto- to nanosecond time-resolved fluorescence and ultrafast transient absorption spectroscopy. The experiments allow one to draw the following conclusions: Charge recombination in a pure donating solvent (DMA) is by no means different from charge recombination in a conventional (unreactive) solvent of otherwise almost identical characteristics, underpinning the pair nature of the recombination process. In particular, the driving force dependence clearly shows Marcus inversion for both types of solvents, and the reaction rates are identical over the entire driving force range studied. Comparison of the time scales for charge separation and charge recombination shows that the former are not only significantly faster than solvation dynamics, but also much faster than the latter. It is also interesting to note that the charge separation rates in pure DMA have been found to be nonexponential, whereas in the present study, we have found almost monoexponential decays for the charge recombination kinetics. Both the difference in time scale as well as the (non)exponentiality can be given a very qualitative explanation based on the ideas of Castner and Vauthey. Charge separation in a pure donating solvent can occur between a vast distribution of fluorophore−quencher pairs with different relative orientations exhibiting different orbital overlap or electronic coupling. However, once the geminate radical ion pair has formed, the optimal "configuration" for charge recombination is not necessarily already at hand. The relative orientation of the reactant pair as well as the solvent will have to reorganize for charge recombination to proceed, necessarily slowing the electron transfer process and making it solvent dependent. As a matter of fact, charge recombination kinetics indeed show a distinct dependence on the solvent dynamics, that is, faster in ACN with a short solvent relaxation time and slower in BA and DMA with longer solvent relaxation times.

To support the qualitative conclusions, we have fitted different models to the experimental data. All models are based on the diffusion-reaction equation approach, differing merely in the assumptions made for the intrinsic electron transfer step of the charge recombination. Obviously, model I, which does not take into account any dynamic solvent effects, is incapable of rationalizing the experimental observation. Likewise, the application of model II, which assumes the immediate generation of the ions in equilibrium and only then assumes intrinsic solvent control of the charge transfer, fails. It requires an electron transfer model III, which, albeit in a very simplistic way, accounts for the generation of the ions in a nonequilibrium configuration and their subsequent solvent-controlled relaxation, to nicely reproduce all of the above-mentioned experimental findings. Nonetheless, we are aware that, to obtain a complete and quantitative account of the experimental processes, it would be necessary to solve the combined energetic (here modeled by a monoexponential decay with characteristic time τ_L) and material diffusion (here indeed completely solved) problem. Additionally, recent experimental findings have shown that

dx.doi.org/10.1021/jp306629v | J. Phys. Chem. A 2012, 116, 9473−9483

most likely even orientational correlation effects are to be taken into account simultaneously.[60]

■ ASSOCIATED CONTENT

Supporting Information

Transient absorption spectrum of pure DMA in the absence of fluorophore. Selected fits from Table 3. This material is available free of charge via the Internet at http://pubs.acs.org.

■ AUTHOR INFORMATION

Corresponding Author

*E-mail: eric.vauthey@unige.ch.

Notes

The authors declare no competing financial interest.

■ ACKNOWLEDGMENTS

This work was supported by the Fonds National Suisse de la Recherche Scientifique through the NCCR MUST and the University of Geneva. A.R. thanks Prof. Eric Bakker and Günter Mistlberger for providing the FluoroLog-3 for emission measurements. A.R. is deeply indebted to Jakob Grilj for setting up the transient absorption.

■ REFERENCES

(1) Marcus, R. A. *J. Chem. Phys.* **1956**, *24*, 966−978.
(2) Marcus, R. A. *J. Chem. Phys.* **1957**, *26*, 872−877.
(3) Efrima, S.; Bixon, M. *Chem. Phys. Lett.* **1974**, *25*, 34−37.
(4) Jortner, J. *J. Chem. Phys.* **1976**, *64*, 4860−4860.
(5) Zusman, L. D. *Chem. Phys.* **1980**, *49*, 295−304.
(6) Sumi, H.; Marcus, R. A. *J. Chem. Phys.* **1986**, *84*, 4272−4272.
(7) Rips, I.; Jortner, J. *J. Chem. Phys.* **1987**, *87*, 2090−2104.
(8) Tominaga, K.; Walker, G. C.; Kang, T. J.; Barbara, P. F.; Fonseca, T. *J. Phys. Chem.* **1991**, *95*, 10485−10492.
(9) Rehm, D.; Weller, A. *Ber. Bunsen-Ges. Phys. Chem.* **1969**, *73*, 834−839.
(10) Rehm, D.; Weller, A. *Isr. J. Chem.* **1970**, *8*, 259−271.
(11) Miller, J. R.; Beitz, J. V.; Huddleston, R. K. *J. Am. Chem. Soc.* **1984**, *106*, 5057−5068.
(12) Wasielewski, M. R. *Chem. Rev.* **1992**, *92*, 435−461.
(13) Gray, H. B.; Winkler, J. R. *Proc. Natl. Acad. Sci. U.S.A.* **2005**, *102*, 3534−3534.
(14) Kestner, N. R.; Logan, J.; Jortner, J. *J. Phys. Chem.* **1974**, *78*, 2148−2166.
(15) Jortner, J.; Bixon, M. *J. Chem. Phys.* **1988**, *88*, 167−170.
(16) Walker, G.; Aakesson, E.; Johnson, A.; Levinger, N.; Barbara, P. *J. Phys. Chem.* **1992**, *96*, 3728−3736.
(17) Mataga, N.; Taniguchi, S.; Chosrowjan, H.; Osuka, A.; Kurotobi, K. *Chem. Phys. Lett.* **2005**, *403*, 163−168.
(18) Gould, I. R.; Moser, J. E.; Armitage, B.; Farid, S.; Goodman, J. L.; Herman, M. S. *J. Am. Chem. Soc.* **1989**, *111*, 1917−1919.
(19) Asahi, T.; Mataga, N. *J. Phys. Chem.* **1991**, *95*, 1956−1963.
(20) Vauthey, E. *J. Phys. Chem. A* **2001**, *105*, 340−348.
(21) Burshtein, A. I. *Adv. Chem. Phys.* **2004**, *129*, 105−418.
(22) Rosspeintner, A.; Kattnig, D.; Angulo, G.; Landgraf, S.; Grampp, G. *Chem.-Eur. J.* **2008**, *14*, 6213−6221.
(23) Dorfman, R. C.; Fayer, M. D. *J. Chem. Phys.* **1992**, *96*, 7410−7410.
(24) Weidemaier, K.; Tavernier, H. L.; Swallen, S. F.; Fayer, M. D. *J. Phys. Chem. A* **1997**, *101*, 1887−1902.
(25) Closs, G. L.; Calcaterra, L. T.; Green, N. J.; Penfield, K. W.; Miller, J. R. *J. Phys. Chem.* **1986**, *90*, 3673−3683.
(26) Staerk, H.; Kuehnle, W.; Weller, A.; Werner, U. *Z. Phys. Chem.* **1995**, *188*, 61−73.
(27) Verhoeven, J. W. *Adv. Chem. Phys.* **1999**, *106*, 603−644.
(28) Nagasawa, Y.; Yartsev, A. P.; Tominaga, K.; Bisht, P. B.; Johnson, A. E.; Yoshihara, K. *J. Phys. Chem.* **1995**, *99*, 653−662.
(29) Saik, V. O.; Goun, A. A.; Fayer, M. D. *J. Chem. Phys.* **2004**, *120*, 9601−9611.
(30) Morandeira, A.; Fürstenberg, A.; Gumy, J.; Vauthey, E. *J. Phys. Chem. A* **2003**, *107*, 5375−5383.
(31) Shirota, H.; Pal, H.; Tominaga, K.; Yoshihara, K. *J. Phys. Chem. A* **1998**, *102*, 3089−3102.
(32) Castner, E. W.; Kennedy, D.; Cave, R. J. *J. Phys. Chem. A* **2000**, *104*, 2869−2885.
(33) Kobayashi, T.; Takagi, Y.; Kandori, H.; Kemnitz, K.; Yoshihara, K. *Chem. Phys. Lett.* **1991**, *180*, 416−422.
(34) Wang, C.; Akhremitchev, B.; Walker, G. C. *J. Phys. Chem. A* **1997**, *101*, 2735−2738.
(35) Seel, M.; Engleitner, S.; Zinth, W. *Chem. Phys. Lett.* **1997**, *275*, 363−369.
(36) Wolfseder, B.; Seidner, L.; Domcke, W.; Stock, G.; Seel, M.; Engleitner, S.; Zinth, W. *Chem. Phys.* **1998**, *233*, 323−334.
(37) Andrews, D.; McFadyen, G.; Beddard, G. *Chem. Phys. Lett.* **1998**, *293*, 343−351.
(38) Engleitner, S.; Seel, M.; Zinth, W. *J. Phys. Chem. A* **1999**, *103*, 3013−3019.
(39) Xu, Q.-H.; Scholes, G. D.; Yang, M.; Fleming, G. R. *J. Phys. Chem. A* **1999**, *103*, 10348−10358.
(40) Ghosh, H. N.; Verma, S.; Nibbering, E. T. J. *J. Phys. Chem. A* **2011**, *115*, 664−670.
(41) Morandeira, A.; Fürstenberg, A.; Vauthey, E. *J. Phys. Chem. A* **2004**, *108*, 8190−8200.
(42) Mattes, S. L.; Farid, S. *J. Am. Chem. Soc.* **1982**, *104*, 1454−1456.
(43) Gardecki, J. A.; Maroncelli, M. *Appl. Spectrosc.* **1998**, *52*, 1179−1189.
(44) Muller, P.-A.; Högemann, C.; Allonas, X.; Jacques, P.; Vauthey, E. *Chem. Phys. Lett.* **2000**, *326*, 321−327.
(45) Duvanel, G.; Banerji, N.; Vauthey, E. *J. Phys. Chem. A* **2007**, *111*, 5361−5369.
(46) Banerji, N.; Duvanel, G.; Perez-Velasco, A.; Maity, S.; Sakai, N.; Matile, S.; Vauthey, E. *J. Phys. Chem. A* **2009**, *113*, 8202−8212.
(47) Iwai, S.; Murata, S.; Katoh, R.; Tachiya, M.; Kikuchi, K.; Takahashi, Y. *J. Chem. Phys.* **2000**, *112*, 7111−7111. Indeed, this reference only reports on CA and DCA, as well as a different TCA isomer. However, we can safely assume that the quenching dynamics of TCA and TriCA will occur on similar time scales, given the driving forces are between those of the TCA isomer and DCA and that there is a clear trend with driving force.
(48) Fita, P.; Luzina, E.; Dziembowska, T.; Radzewicz, C.; Grabowska, A. *J. Chem. Phys.* **2006**, *125*, 184508.
(49) Kattnig, D. R.; Rosspeintner, A.; Grampp, G. *Phys. Chem. Chem. Phys.* **2011**, *13*, 3446−3460.
(50) Neufeld, A. A.; Burshtein, A. I.; Angulo, G.; Grampp, G. *J. Chem. Phys.* **2002**, *116*, 2472−2472.
(51) Goun, A.; Glusac, K.; Fayer, M. D. *J. Chem. Phys.* **2006**, *124*, 084504−084504.
(52) Deutch, J. M.; Felderhof, B. U. *J. Chem. Phys.* **1973**, *59*, 1669−1671.
(53) Nicolet, O.; Vauthey, E. *J. Phys. Chem. A* **2002**, *106*, 5553−5562.
(54) Matyushov, D. V. *J. Chem. Phys.* **2004**, *120*, 7532−7556.
(55) Angulo, G.; Grampp, G.; Rosspeintner, A. *Spectrochim. Acta, Part A* **2006**, *65*, 727−731.
(56) Tavernier, H. L.; Kalashnikov, M. M.; Fayer, M. D. *J. Chem. Phys.* **2000**, *113*, 10191−10191.
(57) Angulo, G.; Kattnig, D.; Rosspeintner, A.; Grampp, G.; Vauthey, E. *Chem.-Eur. J.* **2010**, *16*, 2291−2299.
(58) Gladkikh, V.; Burshtein, A. I.; Angulo, G.; Pages, S.; Lang, B.; Vauthey, E. *J. Phys. Chem. A* **2004**, *108*, 6667−6678.
(59) Gladkikh, V. S.; Burshtein, A. I.; Tavernier, H. L.; Fayer, M. D. *J. Phys. Chem. A* **2002**, *106*, 6982−6990.
(60) Mohammed, O. F.; Adamczyk, K.; Banerji, N.; Dreyer, J.; Lang, B.; Nibbering, E. T. J.; Vauthey, E. *Angew. Chem., Int. Ed.* **2008**, *47*, 9044−9048.

(61) Riddick, J. A.; Bunger, W. B.; Sakano, T. K. *Techniques of Chemistry. Organic Solvents. Physical Properties and Methods of Purification*; Wiley: New York, 1986.
(62) Horng, M. L.; Gardecki, J. A.; Papazyan, A.; Maroncelli, M. *J. Phys. Chem.* **1995**, *99*, 17311−17337.
(63) Sumalekshmy, S.; Gopidas, K. *Chem. Phys. Lett.* **2005**, *413*, 294−299.
(64) Grilj, J. Ultrafast Excited-State Dynamics of Radical Ions in Liquid Solution. Ph.D. thesis, Université de Genève, Geneva, 2011.
(65) Kellett, M. A.; Whitten, D. G.; Gould, I. R.; Bergmark, W. R. *J. Am. Chem. Soc.* **1991**, *113*, 358−359.
(66) Samori, S.; Tojo, S.; Fujitsuka, M.; Lin, J.; Ho, T.; Yang, J.; Majima, T. *J. Chin. Chem. Soc.* **2006**, *53*, 1225−1225.
(67) Fujita, M.; Ishida, A.; Majima, T.; Takamuku, S. *J. Phys. Chem.* **1996**, *100*, 5382−5387.